



In-situ

K C , W , L ,*, L H , C , L , L ,
W , K E , L L , G , T P J

Gemological Institute, China University of Geosciences, Wuhan 430074, PR China
 Hubei Gem and Jewelry Engineering Technology Research Center, Wuhan 430074, PR China
 School of Materials Science and Engineering, Huazhong University of Science and Technology, Wuhan 430074, PR China
 Mechanical Engineering, University of Birmingham, Birmingham B15 2TT, UK
 School of Electrical and Electronic Engineering, Huazhong University of Science and Technology, Wuhan 430074, PR China
 WMG, Materials Engineering Centre, University of Warwick, CV4 7AL Coventry, UK

ARTICLE INFO

Keywords:

T
C
S
C
B

ABSTRACT

C , - (3DG) . H
 (SLM) (3D)
 . G in-situ (CVD) C
 SLM 3DG ff A CVD
 ff . T 3DG/ ff ()
 (EMI) ff 88% 27%
 (SE) 47.8 B 2.7 GH ff P SE 32.3 B EMI ffi-
 T 2-18 GH .
 SLM

1. Introduction

G , sp^2
 (2630 2^{-1}) 1 ,
 (2 10^5 2^{-1} V $^{-1}$ -1)
 (65000 W $^{-1}$ K $^{-1}$) 2 . H , π - π
 (2D)
 ff
 3 . A fi
 C
 (3DG) fi (60.6 $^{-2}$) 4 (699.7%), fi
 (2DG), 4 , 5 , 6,7 ,
 (EMI) 8
 3DG 9 , 10 ,
 . H . F
 ff 13 . S
 ()
 14 . D
 15 . M
 CVD
 16 . B

*C : G I , C U G , W 430074, PR C .
 E-mail address: @ . (.L).

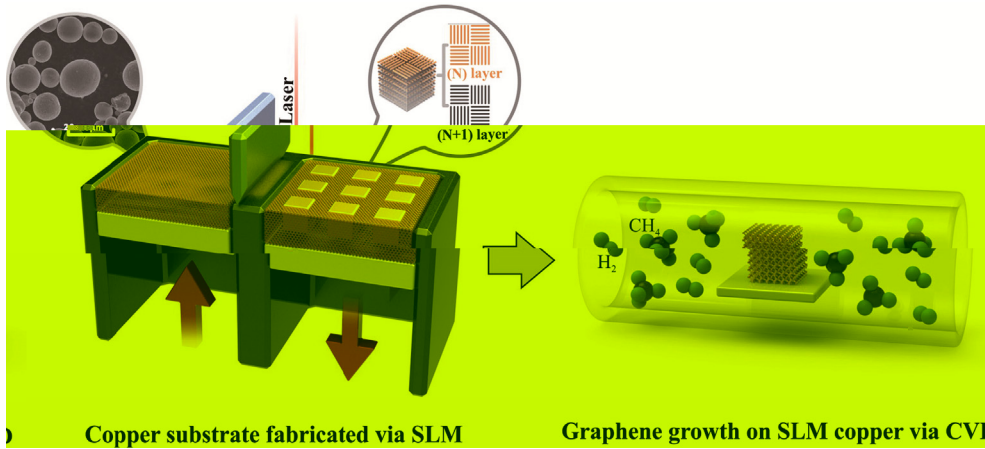


Fig. 1. Schematic of the experimental process. The process involves the fabrication of a copper substrate via SLM, followed by *in-situ* graphene growth on the SLM copper via CVD. The SLM process parameters include laser power and scanning speed. The CVD process parameters include temperature, time, and gas flow rates. The resulting graphene is characterized using Raman spectroscopy and XPS.

ASTM B193-2002
ASTM E1461-2013
LFA (LFA457, G514)
SENTERRA, B311
VNA, A2-18 GH
PNA-N5244A, SE

SLM *in-situ* CVD

LED ($> 800 \text{ J/}$)
LED (400 J/)
LED (130μ)
LED ($27 \text{ E} . 6,$)

(A), 26.7%
(B), 16.7%
(C), 26.7%
(D), D ff

(F . 2)

(C). W
(D),

28 .

3. Results and discussion

3.1. Formation of SLM copper

3.1.1. SLM manufacturing of copper under different line energy densities

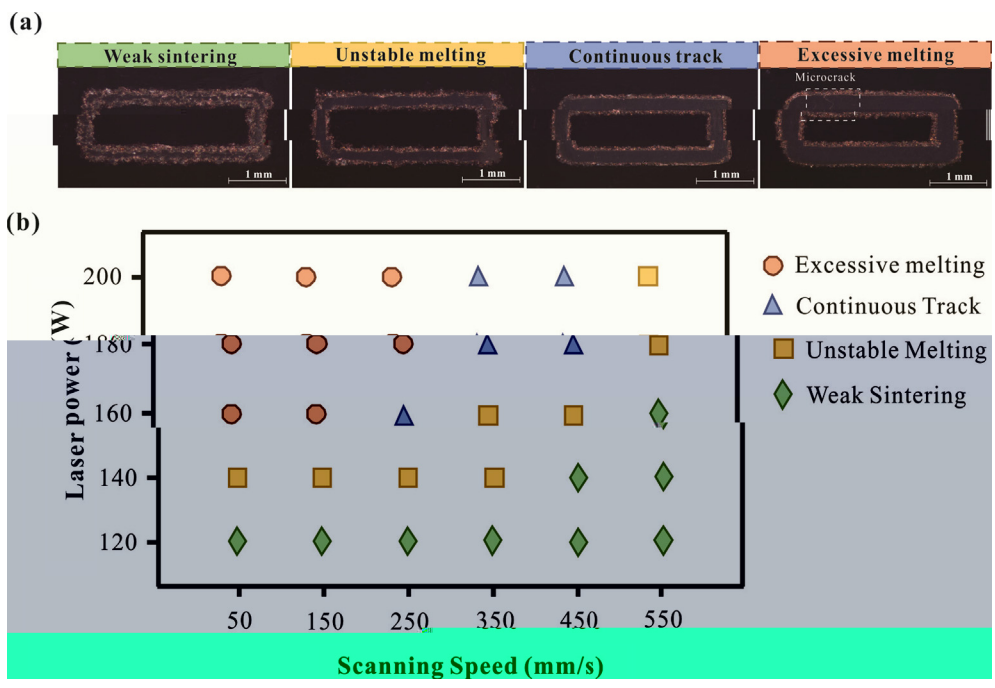


Fig. 2. (a) Optical images of SLM copper tracks under different conditions. (b) Relationship between Laser power and Scanning Speed for different SLM conditions.

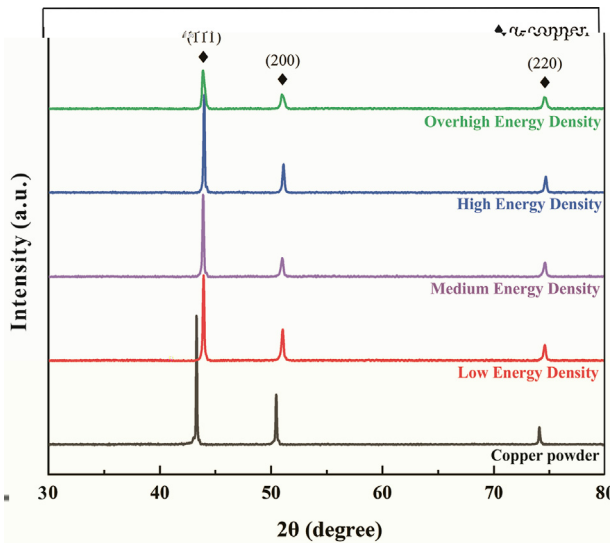


Fig. 3. RD

3.1.2. Formation of anisotropic microstructure under different volumetric energy density

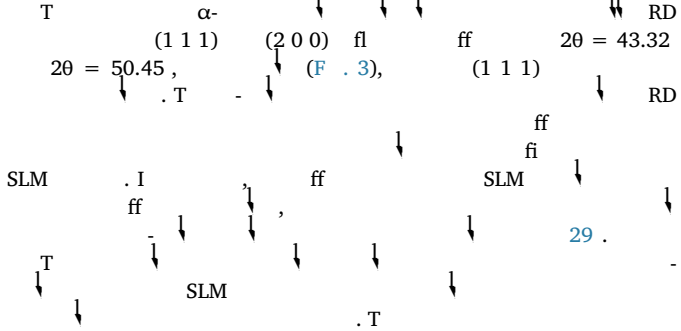


Fig. 4. O

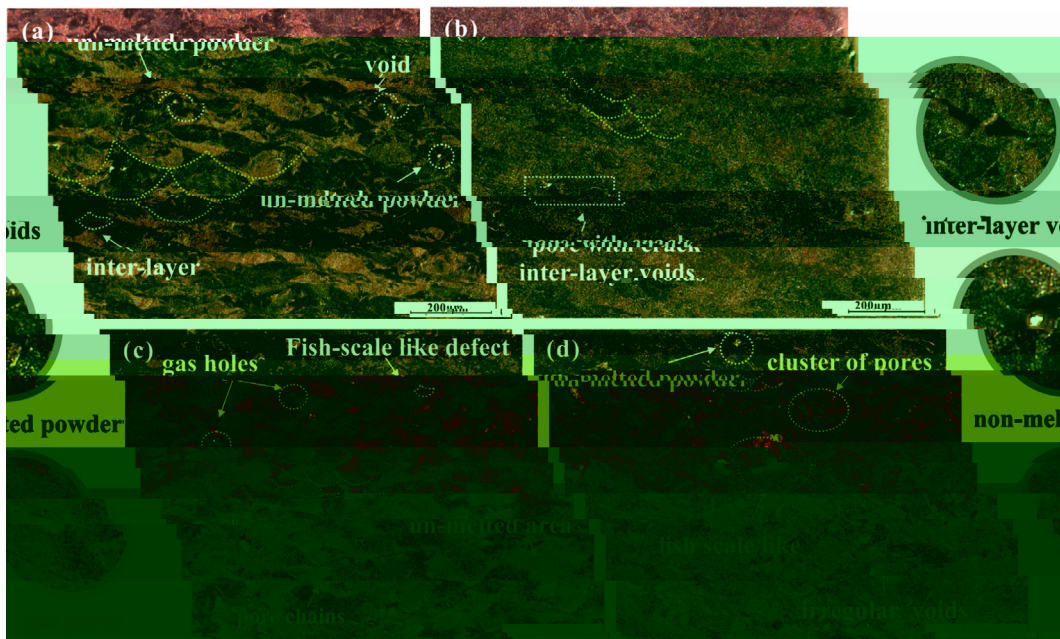


Fig. 4. O (285 J/cm³), (128 J/cm³), (3000 J/cm³), (857 J/cm³)

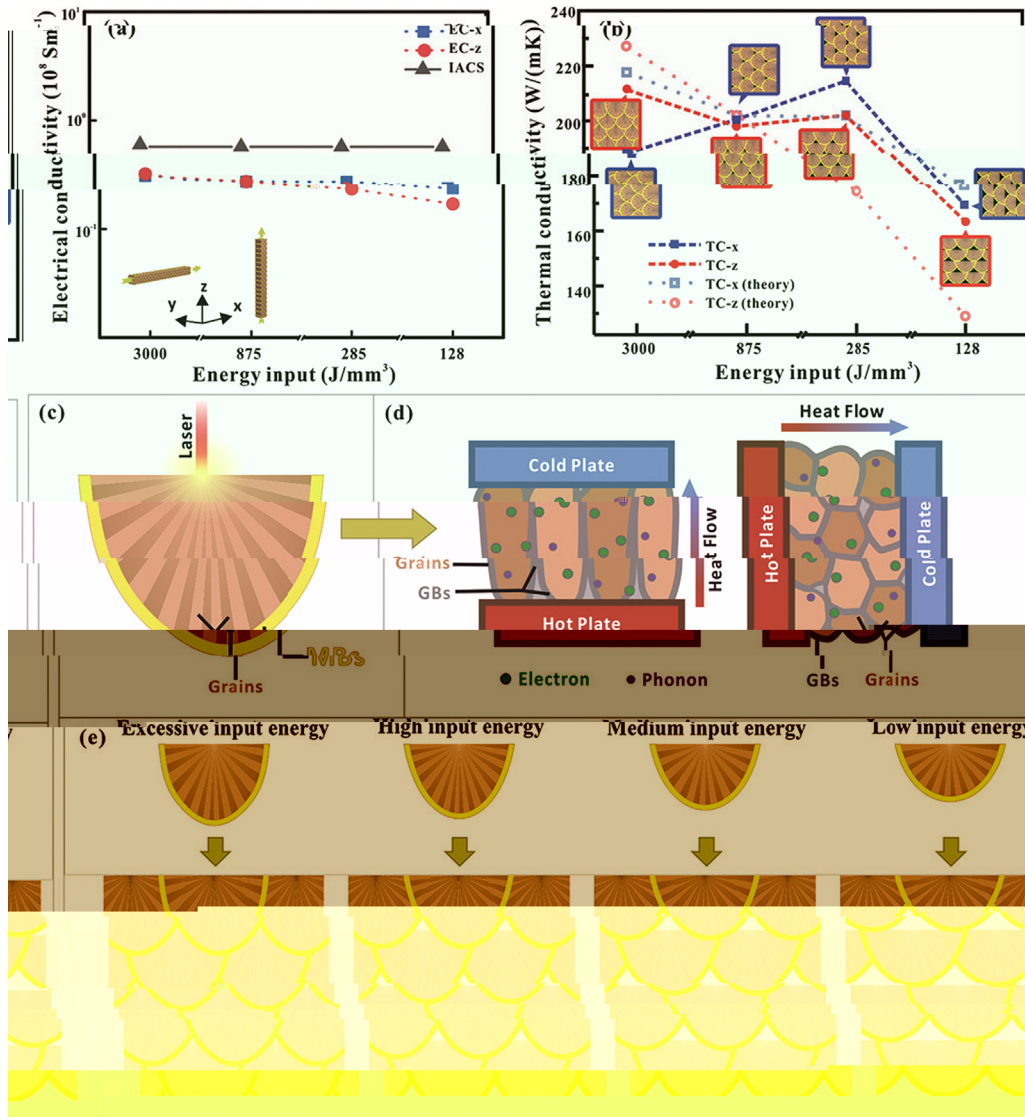


Fig. 7. (a) Electrical conductivity vs energy input. (b) Thermal conductivity vs energy input. (c) Schematic of laser irradiation. (d) Schematic of heat flow. (e) Schematic of grain growth under different energy inputs.

3.3. Morphology and structure of CVD 3DG/Cu porous scaffolds

The morphology and structure of CVD 3DG/Cu porous scaffolds were investigated using SEM, EDS, and XRD. The SEM images (Fig. 8a, b) show the porous structure of the scaffolds, which consists of interconnected 3D graphene (3DG) layers. The EDS analysis (Fig. 8c-d) confirms the presence of carbon and copper in the scaffolds. The XRD patterns (Fig. 8e-g) show the characteristic peaks of 3DG and Cu. The intensity ratio of the D and G bands (I_D/I_G) is used to evaluate the degree of graphitization. The I_D/I_G ratio of the scaffolds is approximately 0.15, indicating a high degree of graphitization. The porous structure of the scaffolds is maintained after the CVD process, as shown in the SEM images (Fig. 8h). The porous structure of the scaffolds is beneficial for the application of the scaffolds in various fields, such as catalysis, energy storage, and tissue engineering.

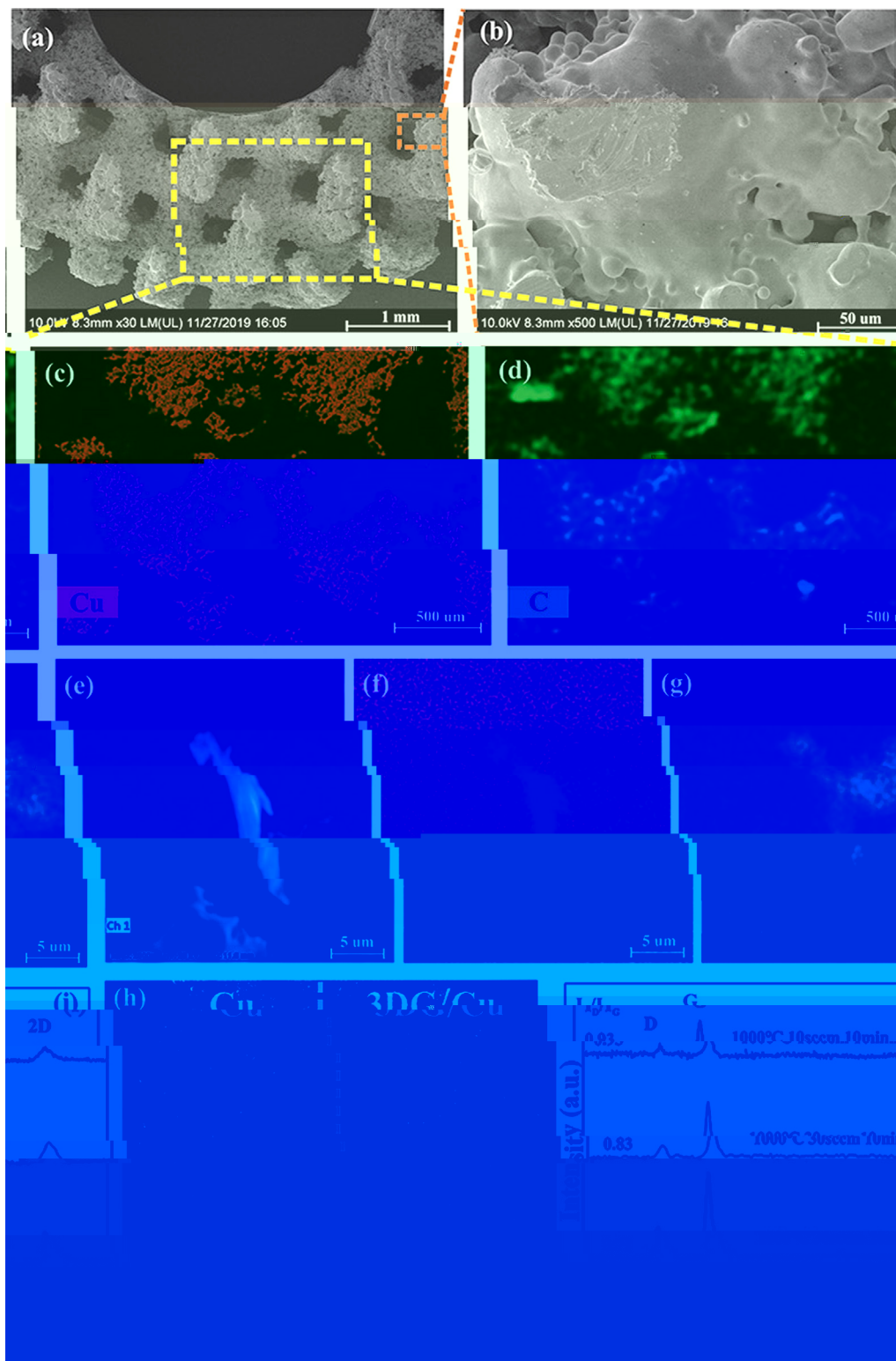


Fig. 8. (a) SEM image of the scaffold at 1 mm scale. (b) High-magnification SEM image of the scaffold at 50 μm scale. (c) EDS map for Cu. (d) EDS map for C. (e) EDS line scan for Cu. (f) EDS line scan for C. (g) EDS line scan for Cu. (h) Raman spectrum of 3DG/Cu showing D and G bands. (i) Raman spectrum of 3DG/C. The Raman spectra show the intensity of the D and G bands, with the G band being significantly more intense than the D band, indicating a high degree of graphitization.

3.4. Thermal property and EMI shielding effectiveness of 3DG/Cu porous scaffolds

The thermal stability of the 3DG/Cu porous scaffolds was evaluated using TGA. The TGA curves show that the 3DG/Cu porous scaffolds exhibit excellent thermal stability, with a weight loss of only 14.8% at 1000 °C. The weight loss is attributed to the decomposition of the 3DG component. The EMI shielding effectiveness of the 3DG/Cu porous scaffolds was also evaluated. The EMI shielding effectiveness of the 3DG/Cu porous scaffolds is 26.8% at 1000 MHz. The EMI shielding effectiveness is attributed to the porous structure of the scaffolds, which provides a large surface area for the absorption and reflection of electromagnetic waves.

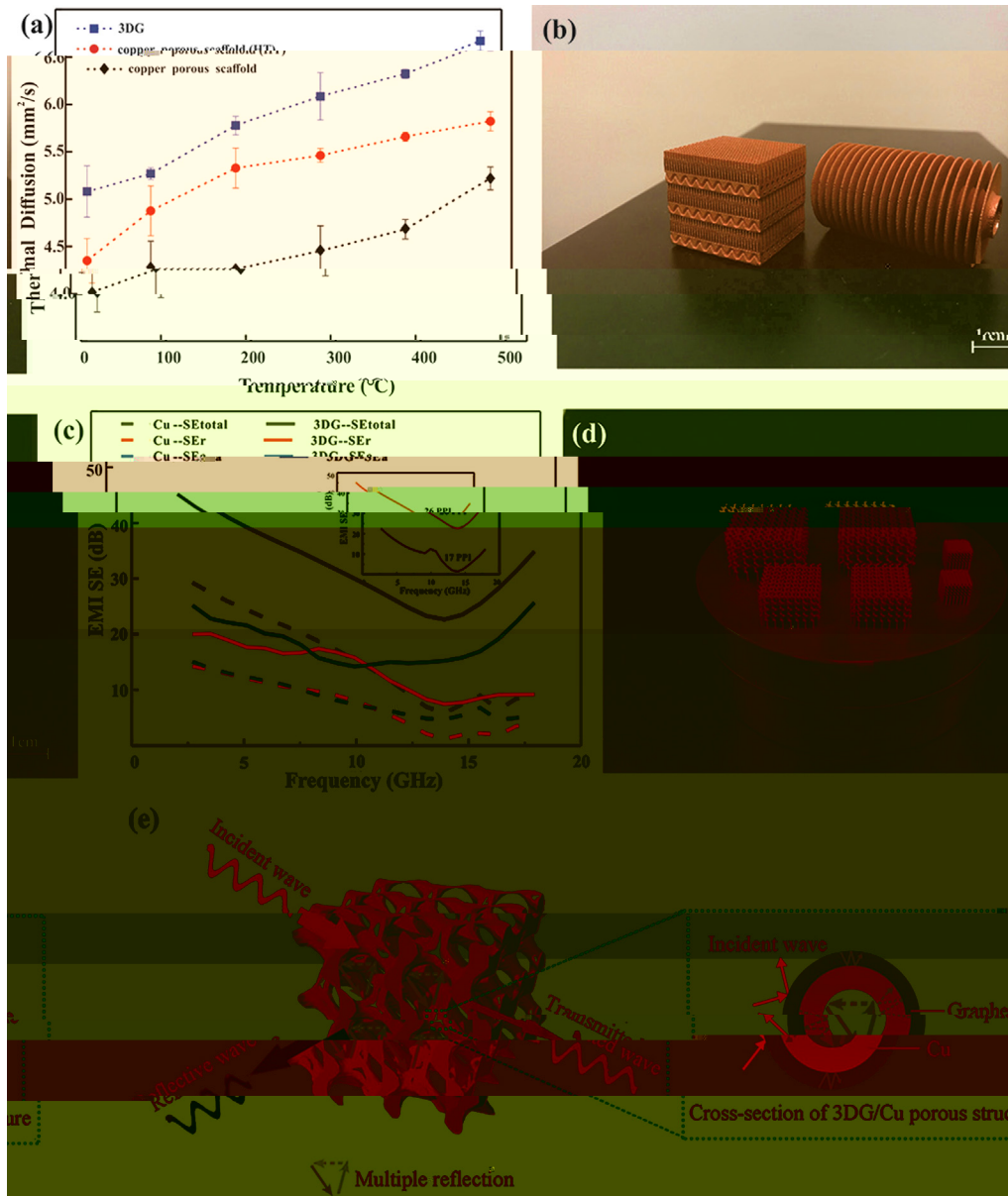


Fig. 9. P 3DG/C ff ; () ff ; () SLM ff ff () S 3DG/C fl EMI. (F

Table 1 C

Coating materials	Substrate	Method	Maximum shielding efficiency (dB)	Improvement of thermal property (%)	Ref
G	G	I + + ↓ + ↓	37	-	50
G	PS	H - ↓ ↓ + ↓ ↓	29.3	-	56
G	PMMA	S ↓ + ↓ +	19	-	57
C /G	/C	A ↓ S fi + ↓ ↓ ↓	-	8.5	58
G	N	F + CVD	-	554	59
G	C -N	H ↓ + ↓ + ↓	20	-	60
G	C	P + CVD	-	2.4	61
G	C	F - + ↓ ↓	47	6.3	62
G	C	CVD + SLM	47.8	27	T

Note: ↓ (↓ ↓)-PPMA, ↓ -PS.

HT
in-situ (F . 9a). S
 3DG/C
 ff
 HT
 1-2
 . I
 fl
 500 μ)
 (F . 9b),
 . G
 (T ↓ 1). I
 N
 T
 EMI, EMI SE,
 (EM)
 2-18 GH (F . 9c),
 ff
 SE
 47.8 B (88.2%)
 3DG/C
 . J K
 133%
 R J V K 45
 . W
 17 26 PPI (F . 9c insert)
 EMI SE. I
 ff
 3DG/C
 32.3 B,
 (30
 3DG/C
 3D
 T
 (SE_a)
 48 . R
 49
 T
 50 . R
 C 51 . F
 52 S O₂ 53 . W

SE_r SE_a
 fi
 F . 9e. W
 3DG/C
 ff
 fl
 3DG/C
 fi
 EM
 fi
 EM
 SE_r. O
 ff
 ff
 J
 54 . I
 fl
 ff . M
 EM
 EM
 . T
 44 . T
 3D
 EM
 CVD
 . I
 R
 S 3.3
 EM
 55 . I
 . O
 3DG/C
 ff
 . T

4. Conclusions

A 3DG/C
in-situ
 ff
 CVD
 T
 ff
 . W
 3DG/C
 EMI SE
 15.9 (
) 32.3 B,
 47.8 B (88.2%)
),
 ff . T 26.8%
 3DG/C
 fl
 . T
 J
 3DG/C
 EMI
 ff

Credit authorship contribution statement

Kaka Cheng: C
 W
 . Yan Li: W
 &
 , F
 R , S
 . Liang Hao: F
 . Chunze Yan:
 R , F
 . Zhaoqing Li: V
 . Zhufeng Liu:
 F ↓ , S
 . Yushen Wang: I
 . Khamis Essa:
 W - & . Li Lee: D
 . Xin Gong: S
 Ton Peijs: W - & , S

53 M 2019;34(5):489-98.
W B, C M, L M. R . A M

54 C H, W S, J , J, C J, S ff F₃O₄
2014;26:3484-9.
2019;121:139-48.
W L, J, Q. T ff MWCNT
-MWCNT . J M S : M B

56 D , P GR, H P, Q F, M B , ML. Effi . J. M
2015;26(3):1895-9.

57 C 2012;22:18772-4.
HB, Q, WG, H , T . ACS A M I

58 S A, U N, T V. T
2011;3:918-24.
M R 2016. :// . /10.1051/ /2016021.

59 P MT, J H, R ff RS, S L. T . N L
2012;12:2959-64.

60 J K, H, H , D . P C -N M L
2017;122:244-7.

61 R H, L S, B S, K TW, L DS, L HJ, T
. S R 2015. :// . /10.1038/ 12710.
T, F SG, L , G Q, L G, R KP, S

62 . M S E A-S 2020. :// . /10.1016/J
.2019.105670.

63 R DA, M LE, M E, H DH, M JL, M BI, . A
N

64 M 2011;59(10):4088-99.
E SF, L KC, S VK, M IC. T . J T
E 1973;1(1):10-38.